15th Triennial World Congress, Barcelona, Spain

VIRTUAL DECOMPOSITION BASED MOTION/FORCE CONTROL OF A KUKA361 INDUSTRIAL MANIPULATOR

Wen-Hong Zhu†* **Joris De Schutter**‡

†*Canadian Space Agency*
6767 route de l'Aeroport, Saint-Hubert, QC J3Y 8Y9, Canada
E-mail: Wen-Hong.Zhu@space.gc.ca

‡*Division of PMA, Department of Mechanical Engineering*
Katholieke Universiteit Leuven
Celestijnenlaan 300B, B-3001 Leuven, Belgium
E-mail: Joris.DeSchutter@mech.kuleuven.ac.be

Abstract: *Virtual decomposition control* is applied to control a KUKA 361 six-joint industrial robot performing hybrid tasks with a rigid unilateral constraint. In order to accommodate motion/force control, the required velocity is re-designed by introducing filtered contact forces in full control dimensions, which makes the controlled robot behave as hybrid controlled for a known contact geometry and impedance controlled for an unknown contact geometry. The real-time experiments demonstrate bouncing-free smooth rigid contact control and asymptotic force tracking results. *Copyright©2002 IFAC*

Keywords: Adaptive control, Force control, Lyapunov stability, Mechanical manipulators, Model-based control, Real-time systems, Robotic manipulators, Robot control, Robot dynamics, Robot kinematics.

1. INTRODUCTION

A systematic approach named "virtual decomposition control" which is able to accomplish a variety of control objectives without restriction on target robotic systems has been proposed by Zhu, *et. al.* (1997). The basic idea is to "cut" an entire robotic system into *objects* and *open chains*. An *object* is typically a rigid body for which the motion/force control specifications are given. An *open chain* is a series of rigid links connected by joints. Thus, the control problem of a complete robotic system is converted into multiple control problems of each subsystem – an *object* or an *open chain*. Structured parametric uncertainties are handled with independent parameter adaptation laws. The dynamic interaction between every two physically connected subsystems is completely represented by a scalar term called *virtual power flow* at the cutting point between them. In this paper, this novel control approach is applied to control a six-joint industrial robot KUKA361 performing hybrid motion/force tasks.

*This work was supported by a Post-Doctoral Fellowship awarded by the Katholieke Universiteit Leuven, Belgium during 1996-1997.

2. VIRTUAL DECOMPOSITION CONTROL

With respect to a particular system - a KUKA361 robot in constrained motion equipped with a SCHUNK force sensor F450/T45 (measurement range of $450N$ and $45Nm$) located at the wrist, see Fig. 1, a "cutting point" is placed at the location of the force sensor such that the robotic system is virtually decomposed into one *object* and one base-fixed *open chain*. The *object* is the end-effector cut from the robot, while the base-fixed *open chain* is the six-joint KUKA361 robot excluding the end-effector. A frame C is assigned and fixed to the "cutting point", and a frame O is fixed to the end-effector.
The dynamic equation of the *object* (the end-effector) is described as (Zhu, *et. al.*, 1997):

$$M_O \frac{d}{dt}({}^O X) + C_O \, {}^O X + G_O = {}^O \underline{F} \,, \qquad (1)$$

where $M_O \in R^{6\times 6}$ is constant and $C_O \in R^{6\times 6}$ is skew-symmetric. The explicit expressions of M_O, C_O, and $G_O \in R^6$ are given by equ. (17) of (Zhu, *et. al.*, 1997), by replacing subscript O_i with O; ${}^O X \in R^6$ denotes a generalized linear/angular velocity of frame O, expressed in frame O; and ${}^O \underline{F} \in R^6$ denotes the net force/moment (including l_{O_i}) expressed in frame O. Since the motion

of the end-effector is constrained with γ dimension, $0 < \gamma < 6$, it follows, in terms of a general modeling approach (De Luca and Manes, 1994), that

$$
\begin{aligned}
{}^{O}X &= T\,\chi\,, && (2)\\
{}^{O}\underline{F} &= {}^{O}U_{C}\,{}^{C}F - Y_m\phi_m - Y_f\varphi_f\,, && (3)
\end{aligned}
$$

where $T \in R^{6\times(6-\gamma)}$ is of rank $6-\gamma$, $Y_m \in R^{6\times(6-\gamma)}$, $Y_f \in R^{6\times\gamma}$ is of rank γ, $\chi \in R^{6-\gamma}$ denotes the independent velocity coordinates, $\phi_m \in R^{6-\gamma}$, and $\varphi_f \in R^{\gamma}$ denotes the independent coordinates of the constraint force; ${}^{O}U_C \in R^{6\times6}$ is a force/moment transformation matrix which transforms a force/moment expressed in frame C to a force/moment expressed in frame O; and ${}^{C}F \in R^6$ denotes the exerting force/moment (from the *open chain* toward the *object*) at the "cutting point" located at the force sensor. Therefore, ${}^{C}F$ is also measurable in this special case.

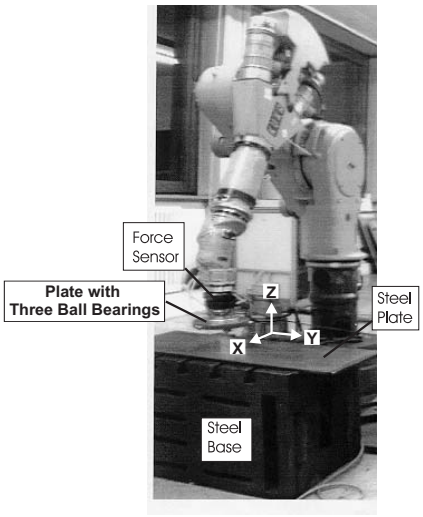

Fig. 1. The KUKA361 robot in contact with the environment.

Remark 2.1: Note that T in (2) replaces $[\ T_K \quad T_D\ ]$ in (De Luca and Manes, 1994). It implies that both pure free motion and motion with dynamic force are handled in a unified manner. Thus, Y_m may contain zero-value columns corresponding to pure free motion. The orthogonality $T^T Y_f = 0$ holds according to equ. (18) of (De Luca and Manes, 1994).

Remark 2.2: In equ. (3), ϕ_m represents the coordinates of the dynamic force, see (De Luca and Manes, 1994). In general, frictional forces, damping and spring forces of a dynamic environment can all be modeled as ϕ_m. Without loss of generality, it is assumed that the mass properties of any dynamic environment have been included into the end-effector such that ϕ_m does not include any inertial force. Thus, ϕ_m is state dependent and can be expressed in terms of linear parameters

$$\phi_m = \mathcal{Y}_m^*\theta_m\,, \qquad (4)$$

where $\mathcal{Y}_m^*$ is a regressor matrix being functions of the measurable states, and θ_m is a corresponding parameter vector. It follows that

$$Y_m\phi_m = \mathcal{Y}_m\theta_m \qquad (5)$$

with $\mathcal{Y}_m = Y_m\mathcal{Y}_m^*$.

A pseudoinverse of Y_f is denoted as $Y_f^{\#}$ such that $Y_f^{\#}Y_f = I_\gamma$. Thus, matrix $[T \quad Y_f^{\#T}] \in R^{n\times n}$ is invertible such that

$$\left[T \quad Y_f^{\#T}\right]^{-1} = \begin{bmatrix} \Omega^T \\ Y_f^T \end{bmatrix}\,, \qquad (6)$$

where $\Omega \in R^{6\times(6-\gamma)}$ is a matrix defined by (6).

After $Y_f^{\#}$ is determined, the velocity vector ${}^{O}X$ can be rewritten as

$${}^{O}X = T\,\chi + Y_f^{\#T}\,\chi_f\,, \qquad (7)$$

where $\chi_f \in R^{\gamma}$ denotes the velocity coordinates associated with the constraints. Note that $\chi_f = 0$ when the constraints hold.

The required net force/moment for the end-effector is designed as

$$
\begin{aligned}
{}^{O}\underline{F}_r &= {}^{O}\underline{F}_r^* + K_O({}^{O}X_r - {}^{O}X)\,, && (8)\\
{}^{O}\underline{F}_r^* &\triangleq \mathcal{Y}_O\hat{\theta}_O + \mathcal{Y}_m\hat{\theta}_m + Y_f\varphi_{fr}\,, && (9)
\end{aligned}
$$

where ${}^{O}X_r$ represents the required vector of ${}^{O}X$, and will be designed in the next section; K_O is a positive-definite gain matrix; $\varphi_{fr} \in R^{\gamma}$ represents the required vector of φ_f; $\hat{\theta}_m$ denotes the estimate of θ_m; and $\hat{\theta}_O$ denotes the estimate of $\theta_O \in R^{13}$ - a parameter vector of the *object* and is governed by

$$\mathcal{Y}_O\theta_O \triangleq M_O \cdot \frac{d}{dt}({}^{O}X_r^*) + C_O \cdot {}^{O}X_r^* + G_O\,. \qquad (10)$$

Note that $\mathcal{Y}_O \in R^{6\times13}$ denotes a regressor matrix, and

$${}^{O}X_r^* \triangleq T\,\chi_r^*\,, \qquad (11)$$

where $\chi_r^* \in R^{n-\gamma}$ denotes a design vector to be specified later.

The detailed expression of θ_O is

$$
\begin{aligned}
\theta_O = [&m_O,\ m_O\,{}^{O}r_x,\ m_O\,{}^{O}r_y,\ m_O\,{}^{O}r_z,\\
&m_O\,{}^{O}r_x^2,\ m_O\,{}^{O}r_y^2,\ m_O\,{}^{O}r_z^2,\\
&m_O\,{}^{O}r_x\,{}^{O}r_y - I_{xy},\ m_O\,{}^{O}r_x\,{}^{O}r_z - I_{xz},\\
&m_O\,{}^{O}r_y\,{}^{O}r_z - I_{yz},\ I_{xx},\ I_{yy},\ I_{zz},]^T\\
&\in R^{13}\,, \qquad (12)
\end{aligned}
$$

where m_O is the mass; ${}^O r = [{}^O r_x, {}^O r_y, {}^O r_z]^T \in R^3$ denotes a vector pointing from the origin of frame O towards the mass center, which is expressed in frame O; I_{xx}, I_{yy}, I_{zz}, I_{xy}, I_{xz}, and I_{yz} are elements of the inertial tensor around the mass center and expressed in frame O. Each element of $\hat{\theta}_O$ is updated by a $\mathcal{P}$ function defined by Zhu and De Schutter (1999) (equ. (4) on page 311) as

$$(\hat{\theta}_O)_j = \mathcal{P}\left((\mathcal{Y}_O)_j^T T(\chi_r^* - \chi), c_{Oj}, (\theta_O)_j^-, (\theta_O)_j^+\right) , \quad (13)$$

where $(\hat{\theta}_O)_j$ denotes the jth element of $\hat{\theta}_O$ and $(\mathcal{Y}_O)_j$ denotes the jth column of $\mathcal{Y}_O$, respectively, $j = 1, \cdots, 13$; $c_{Oj} > 0$ is the update gain; and $(\theta_O)_j^-$ and $(\theta_O)_j^+$ denote the lower and upper bounds of $(\theta_O)_j$ (the jth element of θ_O), respectively. The jth element of $\hat{\theta}_m$ is updated by

$$(\hat{\theta}_m)_j = \mathcal{P}\left((\mathcal{Y}_m)_j^T T(\chi_r^* - \chi), c_{mj}, (\theta_m)_j^-, (\theta_m)_j^+\right) \quad (14)$$

with $c_{mj} > 0$, $(\mathcal{Y}_m)_j$ denotes the jth column of $\mathcal{Y}_m$, and $(\theta_m)_j^-$ and $(\theta_m)_j^+$ denote the lower and upper bounds of $(\theta_m)_j$ (the jth element of θ_m), respectively.

The base-fixed *open chain* is a special form of *open chain* by setting the base velocity to zero. This *open chain* has a total of 6 links and 6 joints. Joint k, $k = 1, \cdots, 6$, connects link $k-1$ with link k (link 0 is fixed to the ground). Frame B_k is fixed to the kth link with its Z axis along the kth joint. The dynamics of the *open chain* are comprised of the dynamics of the rigid links, denoted as ${}^{B_k}\underline{F}$ and characterized by (1) with frame O to be replaced by B_k accordingly, and the dynamics of the joints characterized by

$$\underline{\tau}_k \triangleq I_k^* \cdot \ddot{q}_k + \xi_k(t) + d_k = \tau_k - Z_k^T \, {}^{B_k}F , \quad (15)$$

where $I_k^* \in R$ is the equivalent rotational inertia; $q_k \in R$ is the joint displacement; $\xi_k(t) \in R$ is the frictional force/torque and $d_k \in R$ denotes a constant uncertainty; $\tau_k \in R$ is the joint control force/torque; $\underline{\tau}_k \in R$ is the net force/torque devoted to the joint dynamics; ${}^{B_k}F \in R^6$ denotes the exerting force/moment exerted from link $k-1$ toward link k, expressed in frame B_k; and $Z_k \in R^6$ is a projection vector along the kth joint axis. In this paper, the frictional force takes the form as

$$\xi_k(t) = k_{ck} sign(\dot{q}_k) + k_{vk}\dot{q}_k , \quad (16)$$

i.e. Coulomb and viscous frictions are considered, where $k_{ck} > 0$ and $k_{vk} > 0$ denote the coefficients of Coulomb and viscous frictions, respectively.

Equ. (2) in (Zhu, *et. al.*, 1997) yields ${}^C X = {}^O U_C^T \, {}^O X$, ${}^O X = {}^C U_O^T \, {}^C X$ with ${}^C U_O = {}^O U_C^{-1}$. An invertible Jacobian matrix $J \in R^{6\times 6}$ is defined such that ${}^C X = J\dot{q}$, where $\dot{q} = [\dot{q}_1, \cdots, \dot{q}_6]^T \in R^6$ denotes the joint velocities. Accordingly, the required velocities ${}^C X_r = {}^O U_C^T \, {}^O X_r$ and $\dot{q}_r = J^{-1} \, {}^C X_r = J^{-1} \, {}^O U_C^T \, {}^O X_r$ are obtained. Then, ${}^{B_k}X \in R^6$ and ${}^{B_k}X_r \in R^6$ can be obtained recursively in terms of $\dot{q}$ and $\dot{q}_r$.

The required net force/moment of link k, denoted as ${}^{B_k}\underline{F}_r$, is obtained by applying (8) and (9) without the last two terms in the right hand side of (9), replacing the subscript O with B_k, and replacing ${}^O X_r^*$ with ${}^{B_k}X_r$. This forms $\underline{\mathcal{F}}_r = [0_6^T, {}^{B_1}\underline{F}_r^T, \cdots, {}^{B_6}\underline{F}_r^T]^T \in R^{42}$. Consequently, the required projection force/moments along the joints, denoted as $\mathcal{F}_r^z = [(Z_1^T \, {}^{B_1}F_r), \cdots, (Z_6^T \, {}^{B_6}F_r)]^T \in R^6$, are obtained in terms of the first six rows of equ. (34) of (Zhu, *et. al.*, 1997) by eliminating the subscript j in all terms and setting $l_j = 6$ and $T_j = C$ such that

$${}^{T_j}F_r = {}^C F_r = {}^C U_O \, {}^O \underline{F}_r . \quad (17)$$

Finally, the joint control τ_k, $k = 1, \cdots, 6$, is obtained as

$$\tau_k = \mathcal{Y}_k^J \hat{\theta}_k^J + k_k^J(\dot{q}_{kr} - \dot{q}_k) + Z_k^T \, {}^{B_k}F_r , \quad (18)$$

where $k_k^J > 0$,

$$\mathcal{Y}_k^J = [\ \ddot{q}_{kr} \quad sign(\dot{q}_k) \quad \dot{q}_k \quad 1\ ] , \quad (19)$$

and $\hat{\theta}_k^J$ represents the estimate of θ_k^J defined by

$$\theta_k^J = [\ I_k^* \quad k_{ck} \quad k_{vk} \quad d_k\ ]^T \in R^4 . \quad (20)$$

The $\mathcal{P}$ function is used again to update each (jth) element of $\hat{\theta}_k^J$ in terms of

$$(\hat{\theta}_k^J)_j = \mathcal{P}\left((\mathcal{Y}_k^J)_j(\dot{q}_{kr} - \dot{q}_k), c_{kj}^J, (\theta_k^J)_j^-, (\theta_k^J)_j^+\right) , \quad (21)$$

where $j = 1, \cdots, 4$; $(\mathcal{Y}_k^J)_j$ denotes the jth element of $\mathcal{Y}_k^J$; $c_{kj}^J > 0$ represents the parameter update gain; and $(\theta_k^J)_j^-$ and $(\theta_k^J)_j^+$ represent the lower and upper bounds of $(\theta_k^J)_j$ (the jth element of θ_k^J).

It has been proven (Zhu, *et. al.*, 1997) that the dynamic interaction between the *open chain* and the *object* (the end-effector) can be represented completely by a scalar term named *virtual power flow* at the cutting point, denoted as $-W_C = -({}^C X_r - {}^C X)^T({}^C F_r - {}^C F)$ (see (16) and (40) in (Zhu, *et. al.*, 1997) by setting $W_{B_j} = 0$ and $W_{T_j} = W_C$).

Lemma 1: Consider a single arm constrained robot without kinematic singularity. In view of (3), (8), and (17), it yields

$${}^O X_r - {}^O X \in L_2 \bigcap L_\infty \quad (22)$$

provided that the following inequality holds

$$\begin{aligned} & -({}^O X_r - {}^O X)^T[{}^O \underline{F}_r^* - ({}^O \underline{F} + Y_m \phi_m + Y_f \varphi_f)] \\ \leq \ & -\dot{V}_1 - V_2 , \end{aligned} \quad (23)$$

where V_1 and V_2 are two non-negative continuous scalar functions.

3. REQUIRED VELOCITY DESIGN

In this section, the required velocity ${}^{O}X_r$ will be designed to accommodate motion/force control, while validating (23).

The principle of this design is to make the controlled system behave as hybrid controlled to achieve motion/force tracking in case of a known contact geometry, and behave as impedance controlled to achieve contact stability in case of an unknown contact geometry or unexpected events.

A first order filter is designed to filter the force coordinates

$$\dot{\tilde{\eta}} + C\tilde{\eta} = C \begin{bmatrix} T^T \\ Y_f^{\#} \end{bmatrix} {}^{O}U_C \, {}^{C}F \,, \qquad (24)$$

where $\tilde{\eta} = [\tilde{\eta}_m^T,\ \tilde{\eta}_f^T]^T \in R^6$, with $\tilde{\eta}_m \in R^{6-\gamma}$ and $\tilde{\eta}_f \in R^{\gamma}$; matrix $C = diag\{C_m, C_f\} \in R^{6\times 6}$ is a constant, positive-definite, and diagonal matrix with $C_m \in R^{(6-\gamma)\times(6-\gamma)}$ and $C_f \in R^{\gamma\times\gamma}$.

Remark 3.1: In hybrid tasks, friction is usually involved in the free motion space. The frictional forces are handled in two ways. First, the frictional forces should be incorporated into $Y_m\phi_m$. Second, a properly designed dead-zone should be used to remove the frictional forces from $\tilde{\eta}_m$.

A dead-zone filter with a constant vector $Z \in R^{(6-\gamma)}$, $Z_i \geq 0$ for $i = 1, \cdots, 6-\gamma$, is designed as

$$(\tilde{\eta}_{mz})_i = \begin{cases} (\tilde{\eta}_m)_i - Z_i & (\tilde{\eta}_m)_i > Z_i \\ (\tilde{\eta}_m)_i + Z_i & (\tilde{\eta}_m)_i < -Z_i \\ 0 & \text{otherwise} \end{cases} , \qquad (25)$$

where $(\tilde{\eta}_{mz})_i$ and $(\tilde{\eta}_m)_i$ denote the ith elements of $\tilde{\eta}_{mz}$ and $\tilde{\eta}_m$, respectively, and $\tilde{\eta}_{mz}$ denotes the output of the dead-zone filter.

Finally, the required velocity is designed, in terms of (7), as

$${}^{O}X_r = T(\chi_r - A_m\tilde{\eta}_{mz}) + Y_f^{\#T}(\chi_{fr} - A_f\tilde{\eta}_f) \qquad (26)$$

together with

$$\chi_r^* = \chi_r - A_m\tilde{\eta}_{mz} \,, \qquad (27)$$

where $A_m \in R^{(6-\gamma)\times(6-\gamma)}$ and $A_f \in R^{\gamma\times\gamma}$ are two constant, positive-definite, and diagonal matrices with small elements; $\chi_r \in R^{6-\gamma}$ denotes the required velocity coordinates associated with the free motion; and $\chi_{fr} \in R^{\gamma}$ is a design vector associated with the constraint force.

Remark 3.2: The required velocity designed by Zhu, *et. al.* (1997) takes the form as $T\chi_r$. Thus, the design by (26) can be viewed as a re-design.

In normal circumstances with $\chi_f = 0$, it can be checked that (23) holds by specifying
$\dot{\chi}_{fr} + C_f\chi_{fr} = A_fC_fY_f^{\#\,O}\underline{F}_r^*$,
$V_1 = \frac{1}{2}\Big[(\chi_r^* - \chi)^TT^TM_OT(\chi_r^* - \chi)$
$+(\chi_{fr} - A_f\tilde{\eta}_f)^TC_f^{-1}A_f^{-1}(\chi_{fr} - A_f\tilde{\eta}_f)$
$+\sum_{j=1}^{13}((\theta_O)_j - (\hat{\theta}_O)_j)^2/c_{Oj}$
$+\sum_j((\theta_m)_j - (\hat{\theta}_m)_j)^2/c_{mj}\Big]$, and
$V_2 = (\chi_{fr} - A_f\tilde{\eta}_f)^TA_f^{-1}(\chi_{fr} - A_f\tilde{\eta}_f)$.
It yields

$${}^{O}X_r - {}^{O}X \in L_\infty \bigcap L_2 \,. \qquad (28)$$

Under bounded $\dot{\chi}_r$ and $\dot{\chi}_{fr}$, it follows that (Tao, 1997)

$${}^{O}X_r - {}^{O}X \to 0 \,. \qquad (29)$$

Hence, this leads to

$$\chi_r - \chi - A_m\tilde{\eta}_{mz} \ \to \ 0 \,, \qquad (30)$$
$$\chi_{fr} - \chi_f - A_f\tilde{\eta}_f \ \to \ 0 \,. \qquad (31)$$

Equ. (30) represents a motion tracking equation for both free motion and contact motion involving dynamic force $Y_m\phi_m$. In normal circumstances during free motion, the force coordinates ϕ_m are bounded. By appropriate choice of the dead-zone parameters in (25), zero $\tilde{\eta}_{mz}$ can be obtained. Equ. (30) changes to $\chi_r - \chi \to 0$. This is a velocity tracking equation, where χ_r denotes the required velocity coordinates. Note that position/orientation control can be accomplished by setting $\chi_r = \chi_d + \Lambda\mathcal{E}$, where χ_d denotes the desired velocity coordinates, Λ is a diagonal positive-definite matrix, and $\mathcal{E}$ denotes a term relevant to the position/orientation errors subject to $\int_0^t(\chi_d - \chi)^T\Lambda\mathcal{E}dt \geq -\gamma_0$ with $\gamma_0 > 0$. Two examples in (Zhu, *et. al.*, 1997) show that both linear position errors in $SE3$ and nonlinear orientation errors in $SO3$ satisfy this inequality.

Equ. (31) describes the rigidly constrained motion. In normal circumstances, $\chi_f = 0$, χ_{fr} represents the desired filtered contact force scaled by A_f. In the approach motion with unilateral constraint ($\varphi_{fr} = 0$ in (9)), (31) becomes an approach velocity control equation. Note that χ_f in (31) provides damping to the system, which plays a key role for keeping contact stability during transition phases from approach motion towards constrained motion for unilateral constraints.

4. EXPERIMENTAL RESULTS

A real-time control system consisting of five T800 transputers is used. A sampling frequency of 400Hz is used to calculate the feedback control part, while a sampling frequency of 100Hz is used to calculate all dynamics compensation, parameter adjustment, kinematics, and filtered

force feedback. In the experiments, SI units are used unless otherwise specified.

The KUKA361 robot, illustrated in Fig. 1, weighs 300kg with 8kg payload capacity. The lengths of links 2 and 3 are 0.48m and 0.645m, respectively. Coulomb friction of the first three joints amounts to 40Nm, 35Nm, and 15Nm, respectively.

The three ball bearings located at the end-effector guarantee a planar contact with the 10mm thick steel plate put on a steel base. The X and Y axes lie in the contact plane and the Z axis is normal to the contact plane. During constrained motion, the linear motion along the X and Y axes and the rotational motion around the Z axis belong to the motion space, while the linear motion along the Z axis and the rotational motion around the X and Y axes belong to the constraint space. This yields

$$T = \begin{bmatrix} 1 & 0 & 0 \\ 0 & 1 & 0 \\ 0 & 0 & 0 \\ 0 & 0 & 0 \\ 0 & 0 & 0 \\ 0 & 0 & 1 \end{bmatrix}, \qquad Y_f = \begin{bmatrix} 0 & 0 & 0 \\ 0 & 0 & 0 \\ 1 & 0 & 0 \\ 0 & 1 & 0 \\ 0 & 0 & 1 \\ 0 & 0 & 0 \end{bmatrix},$$

χ represents the linear velocities along the X and Y axes and the angular velocity along the Z axis, and φ_f represents the force along the Z axis and the moments along the X and Y axes. The pseudoinverse of Y_f is chosen as $Y_f^{\#} = Y_f^T$. Thus, it follows that $\Omega = T$. Accordingly, we have $Y_m = T$. The corresponding coordinates ϕ_m represent the frictional force/moments along the motion space spanned by T.

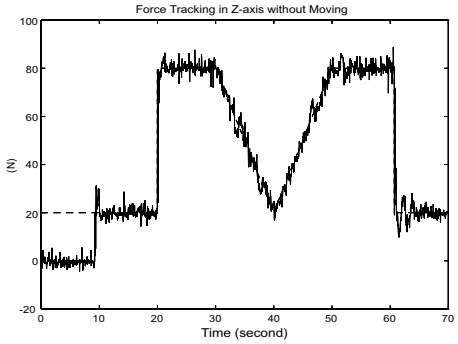

Fig. 2. Force regulation along Z axis with a rigid end-effector.

The experimental results are demonstrated in Fig. 2 to Fig. 6. Fig. 2 shows the force regulation result along the Z axis, when the end-effector with three ball bearings contacts the very rigid steel plate put on a steel base. The force feedback gain and the filter parameter along the Z axis are $A_f = 0.0005$ and $C_f = 8.0$. In Fig. 2, the dashed line denotes the desired force, while the solid line denotes the measured force. The experiment starts by setting the desired force to $20N$. As a result, the robot automatically moves toward the unilateral constraint with an approach speed around $A_f \times 20N \approx 10mm/s$. After the contact is established right before $t = 10s$, a small force overshoot is observed. However, there is no bouncing during the contact. Afterwards, the robot maintains a very good force regulation for both step and ramp inputs.

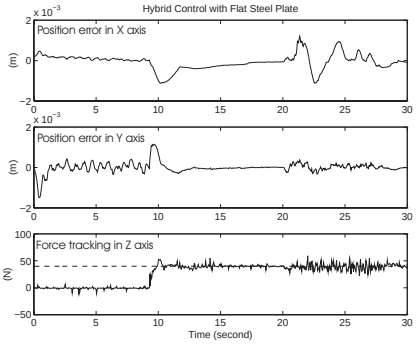

Fig. 3. Hybrid Control of KUKA361 with known contact geometry.

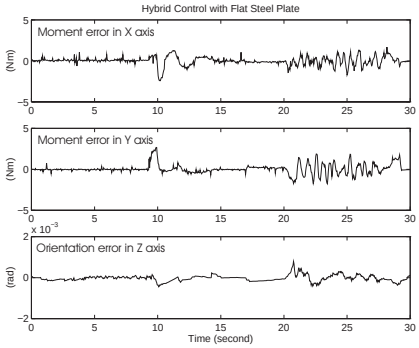

Fig. 4. Hybrid Control of KUKA361 with known contact geometry.

Figs. 3 & 4 show the experimental results for hybrid motion. In the 3 DOF motion space, position/orientation control is accomplished by specifying $\chi_r = \chi_d + \Lambda\mathcal{E}$, where $\Lambda = diag\{3.0, 3.0, 15.0\}$ and $\mathcal{E}$ denotes the position/orientation errors subject to $\dot{\mathcal{E}} = \chi_d - \chi$. The force feedback gains and the filter parameters are $A_f = diag\{0.00025, 0.005, 0.005\}$ and $C_f = diag\{8.0, 10.0, 10.0\}$. Fig. 3 illustrates the position errors in X and Y axes, and the force tracking in Z axis (the dashed line denotes the desired force and the solid line denotes the actual force), respectively. Fig. 4 illustrates the moment errors in X and Y axes, and the orientation error in Z axis, respectively. The robot starts by giving a desired contact force $40N$ in Z axis. The rigid end-effector approaches the steel plate at a speed around $A_{f1} \cdot 40N \approx 10mm/s$. After the contact is established right before $t = 10s$, the actual force in Z axis tracks the desired force precisely and the moment errors in X and Y axes converge to zero quickly. At $t = 20s$, the robot starts to move in Y axis at a speed of $30mm/s$. The motion stops at $t = 27s$. There are small disturbances on the force

tracking and on the moment errors during the motion, due to the very rigid contact. Note that after the contact is established, the force overshoot in Z axis is much smaller than that in Fig 2. This is because a small A_f (0.00025 compared to 0.0005 in Fig. 2) is used in Z axis.

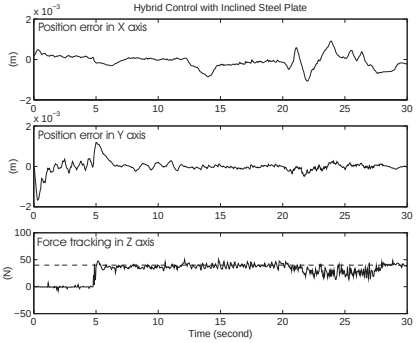

Fig. 5. Hybrid Control of KUKA361 with unknown contact geometry.

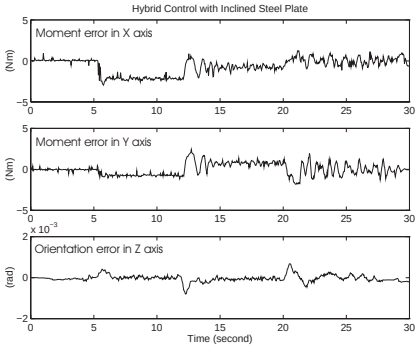

Fig. 6. Hybrid Control of KUKA361 with unknown contact geometry.

Figs. 5 & 6 demonstrate the robustness of the controlled system against geometrical uncertainties. The steel plate is artificially inclined 5.5 deg. around X axis, but this is unknown to the robot. The robot approaches the steel plate as usual. After one rolling bearing contacts the inclined plate ($t = 5s$), there is a constant moment acting on the end-effector ($-2.5Nm$ around X axis). This constant moment changes the orientation of the end-effector automatically until all three rolling bearings are contacting the steel plate ($t = 12s$). This procedure takes about 7 seconds, see Fig. 5. The time period is determined by the inclination angle, the given contact force, and A_f (0.005). When the robot starts to move in Y axis with a speed of $30mm/s$ at $t = 20s$, the contact force in Z axis is lower than the desired value, since the inclined plate results in a non-zero velocity in Z axis.

Remark 4.1: The control parameters to be adjusted are very limited. These parameters include Λ, A_m, C_m, A_f, and C_f. Many other parameters, such as the feedback gains and the parameter adjustment gains, remain unchanged. All the control gains are set approximately to half of their critical values that start to make the system chatter.

Remark 4.2: The robot has $13 \times 6 + 4 \times 6 = 102$ parameters. Each parameter can be updated independently. Since it was very hard to identify these parameters accurately, the upper and lower bounds of those parameters are chosen manually. Some of them may be incorrect. However, the experiments still demonstrate very robust motion/force control results despite of the inaccurate parameters. The estimate of d_j defined by (21) results in a strong integral control against the disturbances and the parameter uncertainties in the joint, and leads to a zero steady error.

Remark 4.3: This paper successfully realized rigid contact control. Compared to a recent publication (Ferretti, *et. al.*, 1998), the proposed controller exhibits smooth transition performance with zero steady tracking error. The success of the smooth rigid contact control and the force regulation is due to the required velocity design which takes advantages of both impedance control (which makes smooth rigid contact control possible) and hybrid control (which makes motion tracking and force regulation possible).

5. CONCLUSION

In this paper, an experimental verification of "virtual decomposition control" has been conducted using a six-joint KUKA361 industrial robot performing hybrid tasks with a rigid unilateral constraint formed by a steel plate put on a steel platform. The experimental results have demonstrated bouncing-free rigid contact control stability and force regulation capability.

REFERENCES

De Luca, A., and C. Manes (1994). Modeling of robots in contact with a dynamic environment. *IEEE Trans. Robotics and Automation*, **10**(3), 542-548.

Ferretti, G., G. Magnani, and A. Zavala Rio (1998). Impact modeling and control for industrial manipulators. *IEEE Control Systems Magazine*, **18**(4), 65-71.

Tao G. (1997). A simple alternative to the Barbălat Lemma. *IEEE Trans. Automatic Control*, **42**(5), 698.

Zhu, W.H., Y. G. Xi, Z. J. Zhang, Z. Bien, and J. De Schutter (1997). Virtual decomposition based control for generalized high dimensional robotic systems with complicated structure. *IEEE Trans. Robotics and Automation*, **RA-13**(3), 411-436.

Zhu, W.H. and J. De Schutter (1999). Adaptive control of mixed rigid/flexible joint robot manipulators based on virtual decomposition. *IEEE Trans. Robotics and Automation*, **15**(2), 310-317.